The Emission Heights of Transition Region Lines in an Equatorial Coronal Hole and the Surrounding Quiet Sun *

Hui Tian[1,2], Li-Dong Xia[3], Jian-Sen He[1], Bo Tan[1] and Shuo Yao[1]

[1] Department of Geophysics, Peking University, Beijing 100871, China; *tianhui924@163.com*
[2] Max-Planck-Institut für Sonnensystemforschung, D-37191 Katlenburg-Lindau, Germany
[3] School of Space Science and Physics, Shandong Univ. at Weihai, Weihai 264209, China

Abstract Using the correlation between the radiance or Doppler velocity and the extrapolated magnetic field, we determined the emission heights of a set of solar transition region lines in an equatorial coronal hole and in the surrounding quiet Sun region. We found that for all of the six lower-transition-region lines, the emission height is about 4–5 Mm in the equatorial coronal hole, and around 2 Mm in the quiet Sun region. This result confirms the previous findings that plasma with different temperature can coexist at the same layer of transition region. In the quiet Sun region, the emission height of the upper-transition-region line Ne VIII is almost the same that of the lower-transition-region line, but in the coronal hole, it is twice as high. This difference reveals that the outflow of Ne VIII is a signature of solar wind in the coronal hole and is just a mass supply to the large loops in the quiet Sun.

Key words: Sun: transition region — Sun: magnetic fields — Sun: solar wind — Sun: UV radiation

1 INTRODUCTION

Solar transition region plays an important role in the origin of the solar wind (e.g. Hassler et al. 1999; Tu et al. 2005a) and in coronal heating (e.g. Hansteen 1993; Feng 2006). Our knowledge of the solar transition region largely depends on EUV (Extreme UltraViolet) spectroscopic observations. Since the plasma is optically thin for most of the EUV emission lines, we can extract information on the physical conditions prevailing in their source regions from the line profiles (for a review see Mariska 1992 and Xia 2003).

Network structure, which is the basic structure in the chromosphere and manifests itself as bright lanes in the radiance images of chromospheric lines, can also be seen in transition region lines (Reeves 1976). The height variation of the network size can be found in Patsourakos et al. (1999) and Tian et al. (2008b). The transition region emission is considered to originate from funnels diverging with height from underlying supergranular boundaries (Gabriel 1976), and low-lying loops with lengths less than 10^4 km (Dowdy et al. 1986). It is further suggested that the funnels can be connected to a solar wind or are just the legs of coronal loops (Peter 2001).

It has been found that most transition region lines are red shifted (see the reviews by Mariska 1992). However, a net blue shift of the upper-transition-region line Ne VIII (λ770) has been observed by the instrument SUMER (Solar Ultraviolet Measurements by Emitted Radiation) on board *SOHO* (Solar and Heliospheric Observatory) (Dammasch et al. 1999). The Doppler shifts of transition region lines seem to have a dependence on the formation temperature (Peter & Judge 1999; Teriaca et al. 1999; Xia et al. 2004).

The Ne VIII line is very useful for investigating the outflows in the upper transition region. In the coronal hole, the blue shift of this line is considered to be a signature of solar wind origin (Peter 1999; Stucki et

---

al. 2000; Wilhelm et al. 2000; Aiouaz et al. 2005; Xia et al. 2003; Hassler et al. 1999; Tu et al. 2005a). While in the quiet Sun, large Ne VIII blue shifts were also found in the network lanes and considered to indicate sources of the solar wind (Hassler et al. 1999) or just mass supply to quiet coronal loops (He et al. 2007; Tian et al. 2008a).

However, disk observations can not provide height information of the radiation and Doppler shift of EUV emission lines, which is very important when investigating the 3-D structure of the transition region (Tu et al. 2005b). Thus, we need to develop a technique to find the heights where certain physical processes dominate. Magnetic field extrapolation is a common way for the solar community to study the magnetic coupling of different solar processes (see e.g. Wiegelmann & Neukirch 2002). With the assumption that the magnetic field may be considered as almost force-free at heights of about 400 km above the photosphere (Metcalf et al. 1995), we have successfully combined the force-free model proposed by Seehafer (1978) and the EUV observations to study the plasma radiation and flows in the quiet Sun and in the coronal hole (Wielgelmann et al. 2005; Tu et al. 2005a,b; Marsch et al. 2004, 2006; He et al. 2007; Tian et al. 2007, 2008a,b).

Tu et al. (2005a,b,c) introduced the concept of correlation height of the source of an EUV emission line. They calculated at different heights the correlation coefficient between the 2D distribution of the line intensity or Doppler shift, and the 2D distribution of the vertical component of the extrapolated magnetic field. The height at which the correlation coefficient reaches its maximum was called the correlation height of the radiation. A possible correlation between the magnetic field and the plasma density (expressible as the square root of an emission-line intensity as a first order approximation) may also be expected from the theoretical point of view that the heating flux density (being proportional to the density) entering the loops is proportional to the magnetic field strength (Marsch et al. 2006; Schrijver et al. 2004).

By using this method, Marsch et al. (2006) determined the emission heights of 12 emission lines with formation temperatures from 7.4×10^3 K to 3.0×10^5 K, in a polar coronal hole region. They found a subregion with strong emission located at lower heights, whereas the weak emission appeared to originate at higher heights. The results suggest that the transition region is highly structured and that plasmas of different temperatures can coexist at the same height in the coronal hole.

However, such correlation analysis has not been applied to an equatorial region. In this paper, we analyze a different data set observed in an equatorial coronal hole region and the surrounding quiet Sun region, and determine the correlation height of each EUV line included in the observation for the two regions. Our data set covered six strong lower-transition-region lines and an upper-transition-region line, Ne VIII. Thus, we can provide a direct comparison of the emission heights of transition region lines in the coronal hole and the quiet Sun.

2 OBSERVATIONS AND DATA REDUCTION

The SUMER data (Wilhelm et al. 1995; Lemaire et al. 1997) analyzed in this paper was obtained from 1997 March 7, 18:00 UT to March 8, 17:42 UT. During this period, SUMER observed an equatorial coronal hole and the surrounding quiet Sun. The slit 2 ($1'' \times 300''$) was used in this observation and kept at a fixed position centered at solar coordinates $X = 0''$ and $Y = 279''$. No compensation for the solar rotation was applied, so the scanning was done by the solar rotation over this period. Since the speed of solar rotation at the pointing position ($X = 0''$, $Y = 279''$) is about $10''$ per hour, the scan covered an area of about $235'' \times 300''$. The white rectangle in Figure 1 shows the scanned area in an EIT (Extreme Ultraviolet Imaging Telescope) image (Fe IX/X) taken on 1997 March 8, 07:00:13 UT. The selected spectral windows covered six lower-transition-region lines and one line (Ne VIII) formed in the upper transition region: see Table 1. We adopt the values of rest wavelength given in the Chianti data base, and the formation temperature given in Xia (2003) and the Chianti data base (Dere et al. 1997; Landi et al. 2006). In each spectral window, 50 spectral pixels (about 2 Å) were transmitted during the 90 s exposure time. This data set has already been analyzed by Lemaire et al. (1999) to study the difference of line broadening in the coronal hole and quiet Sun, and by Aiouaz et al. (2005) and Aiouaz (2008) to check the variation of line shift from the network cell to the network center. More information about this observation can be found in the literature.

The standard SUMER procedures for correcting and calibrating the data were applied, which include local gain correction, flat-field correction, geometrical distortion and dead-time correction. We also averaged the data over four exposures, which greatly improved the signal-to-noise ratio and produced a new data
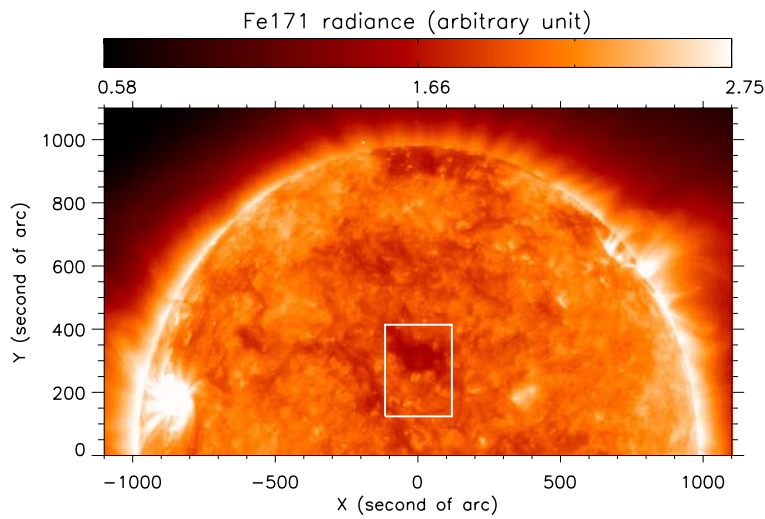
Fig. 1 EIT image (Fe IX/X 171 Å) taken on 1997 March 8, 07:00:13 UT. The area scanned by SUMER/*SOHO* is outlined by the white rectangle.
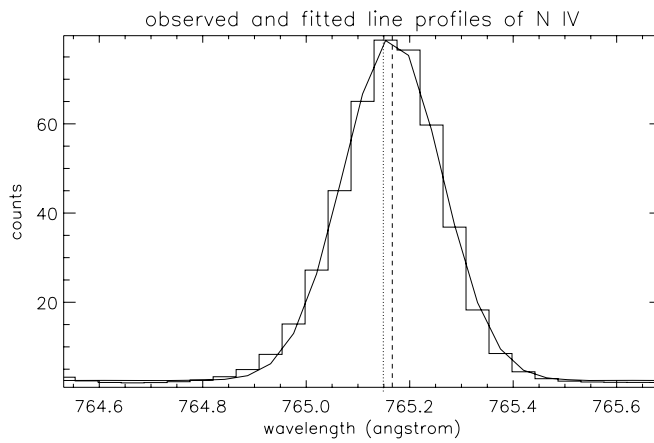

Fig. 2 Observed (histogram) and fitted (smooth line) line profiles of N IV. The dotted and dashed vertical lines indicate the positions of the rest wavelength and the center of the fitted profile, respectively.

Table 1 Emission Lines Used in This Study

Ion	Rest Wavelength (angstrom)	Formation Temperature (log K)	Average Doppler Shift (km s^{-1})
Ne VIII	770.428	5.80	–2.5
O V	760.446	5.35	7
O IV	787.710	5.23	9
O IV	790.199	5.23	9
S V	786.470	5.26	9
N IV	765.149	5.15	7
N III	764.351	4.90	7

set with a pixel size of about $0.95''$ in the direction of solar X. This new pixel size is almost the same as the slit width so that the adjacent data of the new set after average are approximately detected from different positions in the direction of solar X. Along the slit the pixel size corresponds to 1.02 arcsecond (Lemaire et al. 1999). Thus the pixel size was almost the same at solar X and solar Y after this binning.

Each observed spectrum was fitted by a single Gaussian curve, plus a constant and a linear term describing the background. Figure 2 shows the observed line profile of N IV averaged over the whole region (histogram) and a fitting to it (smooth line). The dotted vertical line indicates the position of the center of the fitted profile. The line-of-sight velocity of the plasma can be inferred by using the Doppler shift formula $v_{\rm los} = c(\lambda - \lambda_0)/\lambda_0$, λ_0 being the rest wavelength, and λ, the observed wavelength of the line (the central position of the fitted profile in our case), and c, the speed of light in vacuum. The Doppler velocity of N IV shown in Figure 2 is estimated to be 7 km s^{-1}. The intensity can be calculated by integration over the spectrum. Figure 3 shows the intensity images in N IV and Ne VIII. The boundary of the coronal hole, indicated by the blue dashed line, was determined by hand after an inspection of the intensity image of Ne VIII as well as the EIT Fe IX/X image. This boundary line is almost the same as that used in Aiouaz et al. (2005) so that our results and theirs can be directly compared. It is clear that the dark part of the Ne VIII intensity image can be well outlined by the boundary line. The contours in the left panel represent bright emission of N IV, which clearly outline the network boundaries.

We also estimated the spectral line shift caused by thermal deformations of the optical system of SUMER, which was discussed in Dammasch et al. (1999), by averaging the residual line centroid positions across the north-south extension of the slit. Also, the Doppler shift induced by solar rotation was taken into account by calculating the line-of-sight velocities for all pixels as a function of their nominal mapping onto the solar disk (Dammasch et al. 1999). We removed these two effects before determining the Doppler shifts of the spectral lines.

There are no chromospheric lines in the spectral windows, so we can not carry out an absolute wavelength calibration by using a cold line. Instead, we followed the method adopted by Aiouaz et al. (2005), and assumed a mean value of the doppler shift for each line over the whole observation region. We took the values from Xia (2003), in which the results were based on a statistical study. Table 1 lists the value for each line, negative for blue shifts, positive for red shifts.

Since the SUMER observation lasted for almost 24 hours, during which the magnetic network might have changed a lot, we can not compare a single magnetogram with the SUMER images. During the time of the SUMER observation, 15 full-disk magnetograms were taken by MDI (the Michelson Doppler Imager) on board *SOHO*, every 96 minutes (Scherrer et al. 1995). The average magnetic flux density in the MDI magnetograms needs to be corrected (Berger & Lites 2003; Wang et al. 2003). A factor of 1.6 is used for this correction (Tu et al. 2005a,b). We selected 15 slices taken respectively from the MDI magnetograms observed at 15 different times during the SUMER raster scan, with each slice corresponding to a slice of the SUMER images. The 15 slices were pieced together to reconstruct a new magnetogram with a size of about $235'' \times 2000''$. Then we carried out cross correlation between the intensity image of N IV and this new magnetogram by shifting the magnetogram in the direction of solar Y to obtain an optimal match. After that we chose the data of the magnetic field from the same area as the SUMER image. The resulting magnetogram is shown in Figure 4. A varying noise level can be seen in the magnetogram because the signal-to-noise ratio changes from time to time for the MDI observations, but this will not affect too much of our results since we are mainly interested in the strong magnetic field fluxes.

3 CORRELATION BETWEEN LARGE PHOTOSPHERIC MAGNETIC FLUXES AND LARGE RADIANCES/DOPPLER SHIFTS

In Aiouaz et al. (2005), a three-step filtering was carried out for a Lyman continuum intensity image, which removed the local brightenings and reduced the intensity contrast between the network and internetwork region. Here we applied a similar technique to the intensity images of transition region lines. For each intensity image, we first carried out a median filter of the image. The width of the median filter was chosen as $30''$, corresponding to the mean size of a network cell. The original intensity image was then divided by the median filtered one. Finally the resulting image was smoothed over $10''$, which is the usual accepted value of the network size at transition region temperatures (Patsourakos et al. 1999).
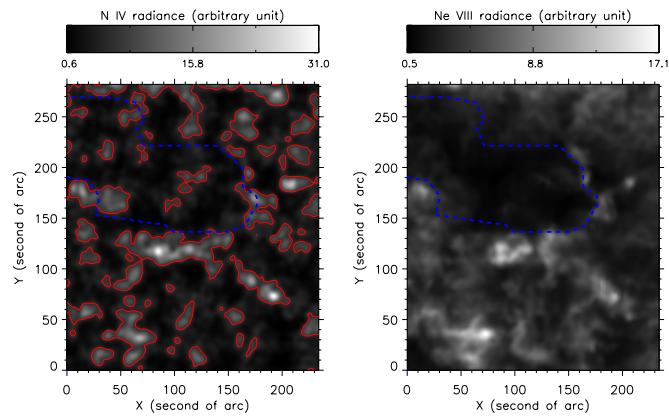
Fig. 3 Intensity images of N IV (left) and Ne VIII (right) in linear scale. The boundary of the coronal hole, indicated by the blue dashed line, was determined by hand and is almost the same as that used in Aiouaz et al. (2005). The contours in the left panel represent patches with large N IV intensity (larger than 6).
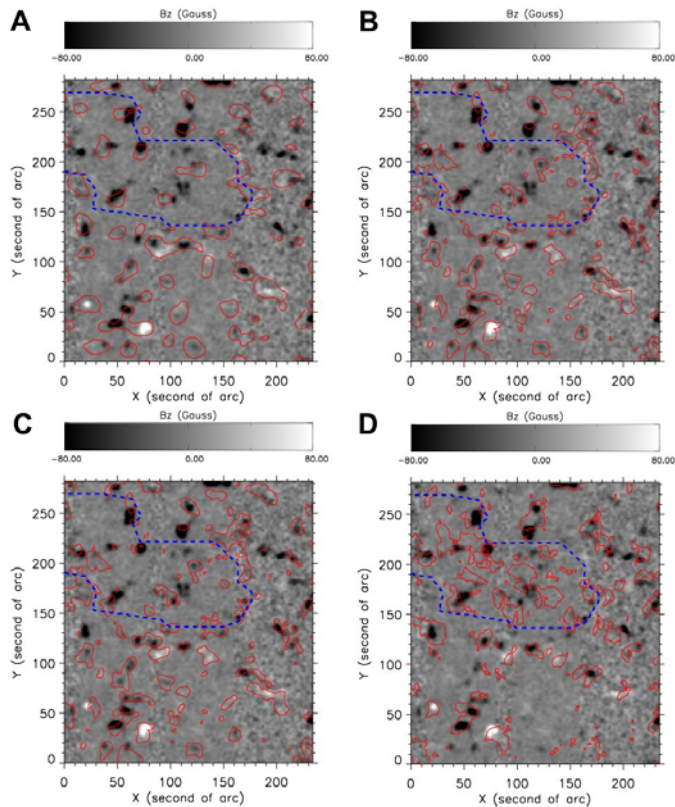

Fig. 4 Magnetogram reconstructed by piecing together 15 slices taken respectively from MDI magnetograms observed at 15 different times during the SUMER raster scan. The thick blue dashed line outlines the boundary of the equatorial coronal hole and the surrounding quiet Sun. The red contours represent bright patches seen on the filtered intensity image (upper) and patches with large shift seen on the dopplergram (lower) for N IV (left) and Ne VIII (right). The contour level of the Doppler shift is 10 km s^{-1} (red shift) for N IV, and –5 km s^{-1} (blue shift) for Ne VIII.

By using this method, we obtained a filtered intensity image for every emission line. The red contours in the upper panels of Figure 4 represent patches of strong emission seen on the filtered image for N IV and Ne VIII respectively. We also added contours of Doppler shift of N IV (larger than $10\,\mathrm{km\,s^{-1}}$) and Ne VIII (smaller than $-5\,\mathrm{km\,s^{-1}}$) on the magnetogram in the lower two panels of Figure 4 respectively. Here a positive value of Doppler shift means an inflow and a negative one, an outflow. Since the intensity images and Dopplergrams of all the six lower-transition-region lines are similar, we only show the results of the N IV line in the figure.

It has long been known that the network structure is the dominant feature in the intensity images of transition region lines. In the upper left panel of Figure 4, the strong intensities and magnetic field concentrations coincide well for the lower-transition-region line N IV in both the coronal hole and the quiet Sun region: this has been well known for decades. While for the Ne VIII line formed in the upper transition region, this coincidence almost disappears in the coronal hole, while remaining obvious in the quiet Sun region. This result is consistent with our previous finding that the network structure is still present in the image of Ne VIII in the quiet Sun region and can hardly be discerned in the coronal hole (Tian et al. 2008b). It suggests that magnetic structures expand more strongly in the coronal hole than in the quiet Sun.

The coincidence between strong red shift of the lower transition region line and magnetic flux concentrations is also obvious in the lower left panel of Figure 4. We calculated the correlation coefficient between the magnetic field strength and the Doppler shift of N IV, and found that this correlation is weaker than that between the magnetic field strength and the intensity of N IV, especially in the coronal hole.

A comparison between the two right panels of Figure 4 reveals a better correlation between the strong magnetic field strength and the large blue shift of Ne VIII. This confirmed our previous results (Tu et al. 2005a,b). In the quiet Sun region, patches of large Ne VIII blue shift tend to coincide with strong magnetic fluxes, which indicates outflows locate at lower part of coronal loops. However, we found the patches of large Ne VIII blue shift are larger in size and closer to each other in the coronal hole, revealing strong outflows to occur at higher layers above the photosphere, that are very likely to be associated with coronal funnels. This direct comparison suggests that the blue shift of Ne VIII has different physical implications, namely an indication of solar wind outflow in the coronal hole (Peter 1999; Stucki et al. 2000; Wilhelm et al. 2000; Aiouaz et al. 2005; Xia et al. 2003; Hassler et al. 1999; Tu et al. 2005a) and just mass supply to the coronal loops in the quiet Sun (He et al. 2007; Tian et al. 2008a).

4 EMISSION HEIGHTS OF TRANSITION REGION LINES

In our present study we used the force-free-field extrapolation method as proposed by Seehafer (1978) to extrapolate the photospheric magnetic field to $40\,\mathrm{Mm}$ above the photosphere. We adopted a value of 0 for the α parameter, corresponding to a potential field. We defined field lines reaching higher than $40\,\mathrm{Mm}$ to be open lines, which were found to be mainly located in the coronal hole. The suitability of this method for our study can be found in Tu et al. (2005b) and thus will not be addressed here.

Figure 5 shows the absolute magnitudes of the vertical component of magnetic field as extrapolated to $4\,\mathrm{Mm}$ (left) and $39\,\mathrm{Mm}$ (right). The contours which are taken from Figure 3 represent bright emission of N IV. Notice that the coincidence between bright emissions of N IV and magnetic concentrations is much better at $4\,\mathrm{Mm}$ than at $39\,\mathrm{Mm}$. This can be further demonstrated by using the correlation analysis described below.

Then we carried out a correlation analysis of the extrapolated magnetic field with the intensity of each lower transition region line, and with Doppler shift of Ne VIII, following the way described in Tu et al. (2005a,b). For each of the lines, we calculated the correlation coefficient between the radiance/Doppler shift and the vertical component of the extrapolated magnetic field ($|B_z|$) at different heights, and identified the height of maximum correlation coefficient as the correlation height.

The reason why we used the vertical component is that the observed Doppler shift is the line-of-sight component of the actual shift, and for the equatorial coronal hole and the surrounding quiet Sun region, the vertical (radial) direction deviated little from the line-of-sight.

Figure 6 shows the height variations of the correlation coefficients of N IV and Ne VIII in the coronal hole and quiet Sun. In the coronal hole region, there are 15018 data points, for which the critical value of the linear correlation coefficient is 0.02 at 99% confidence, and in the quiet Sun region, there are 51525 data points, for which the critical correlation coefficient is 0.01 at the same confidence. The y-axis on the
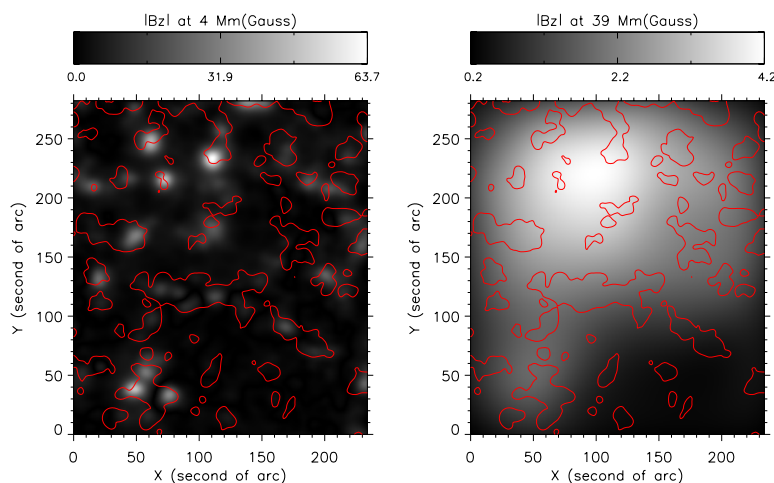
Fig. 5 Extrapolated magnetograms at 4 Mm (left) and 39 Mm (right). The contours taken from Fig. 4 represent bright emission of N IV.
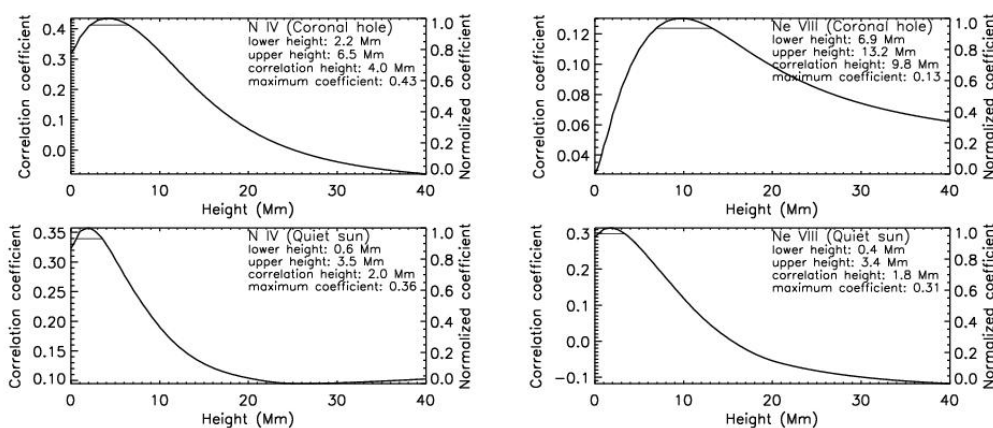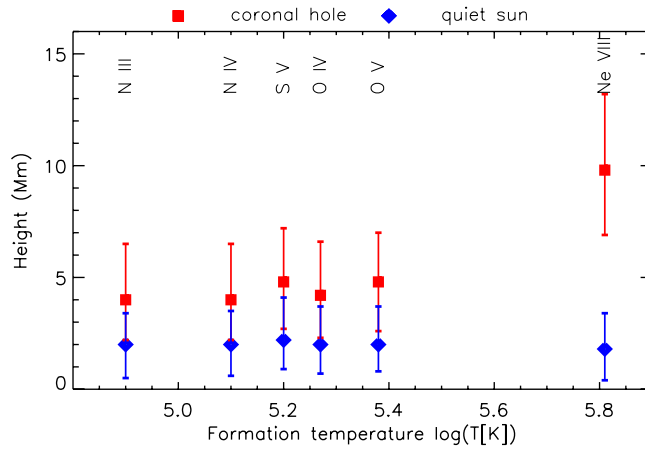

Fig. 6 Height variations of the correlation coefficient between the radiance of N IV and $|B_z|$ (left), and between the blue shift of Ne VIII and $|B_z|$ (right), in the coronal hole (upper) and the quiet Sun (lower). The horizontal bars show the height ranges in which the coefficients are above 95% of the maxima. The y-axis on the right side of each sub-figure indicates the normalized coefficient.

right side of each sub-figure indicates the normalized coefficient, which is obtained by using the formula $\frac{C-C_{\min}}{C_{\max}-C_{\min}}$, where C is the correlation coefficient, $C_{\min}$ and $C_{\max}$ are the minimum and maximum values of the correlation coefficients in each region. In both the coronal hole and quiet Sun region, the correlation coefficient clearly increases with the height to a maximum then decreases, this behavior has already been found for the transition region lines C IV and Ne VIII in Tu et al. (2005a, b). In Figure 6 the horizontal bar shows the height range in which the coefficient is above 95% of its maximum. The maximum correlation coefficient, correlation height, and height range in which the coefficient is above 95% of its maximum are listed in Table 2.

Our result shows that for the six lower-transition-region lines, the correlation heights are 4–5 Mm in the coronal hole, and around 2 Mm in the quiet Sun region. Our result for the quiet Sun region is almost the

Table 2 Correlation Heights and Height Ranges for which the Coefficients are above 95% of the Maxima

Ion	Coronal hole			Quiet Sun		
	Maximum correlation coefficient	Correlation height(Mm)	Height range in which the coefficient is above 95% of its maximum (Mm)	Maximum correlation coefficient	Correlation height(Mm)	Height range in which the coefficient is above 95% of its maximum (Mm)
Ne VIII	0.13	9.8	6.9–13.2	0.31	1.8	0.4–3.4
O V	0.46	4.8	2.6–7.0	0.40	2.0	0.8–3.7
O IV (λ787.710)	0.47	4.2	2.3–6.6	0.38	2.0	0.7–3.7
O IV(λ790.199)	0.46	4.2	2.4–6.7	0.37	2.0	0.6–3.5
S V	0.52	4.8	2.7–7.2	0.44	2.2	0.9–4.1
N IV	0.43	4.0	2.2–6.5	0.36	2.0	0.6–3.5
N III	0.48	4.0	2.2–6.5	0.36	2.0	0.5–3.4

Fig. 7 Temperature variations of the correlation heights in both the quiet Sun and the coronal hole. Squares and diamonds represent the correlation heights and bars indicate the height ranges of emissions.

same as the result for the bright subregion in Marsch et al. (2006), (2–3 Mm), and the correlation height we derived for the coronal hole is lower than that of the dark subregion (9–12 Mm) and higher than that of the bright subregion (2–3 Mm) in the polar coronal hole in Marsch et al. (2006). The latter result seems to be an average effect of the whole coronal hole. Another possible reason may be that the observed line-of-sight component of magnetic field is not exactly in the radial direction in polar regions (Marsch et al. 2006), while in our case the observed magnetic field is almost exactly the radial component since our data refer to near the equator. This result, together with our previous results for a polar coronal hole (Tu et al. 2005a) and for the mid-latitude quiet Sun (Tu et al. 2005b), suggests that the transition region in the coronal hole is higher than in the quiet Sun.

The correlation height and height range of Ne VIII emission show no systematic difference from those of the lower transition region lines in the quiet Sun, but it is totally different from those of the lower-transition-region lines in the coronal hole. This difference clearly reflects the different magnetic structures in the quiet Sun and the coronal hole, and once again supports our conclusion that large blue shift of Ne VIII is an indication of solar wind outflow in the coronal hole (Peter 1999; Stucki et al. 2000; Wilhelm et al. 2000; Aiouaz et al. 2005; Xia et al. 2003; Hassler et al. 1999; Tu et al. 2005a) and is just mass supply to coronal loops in the quiet Sun (He et al. 2007; Tian et al. 2008a).
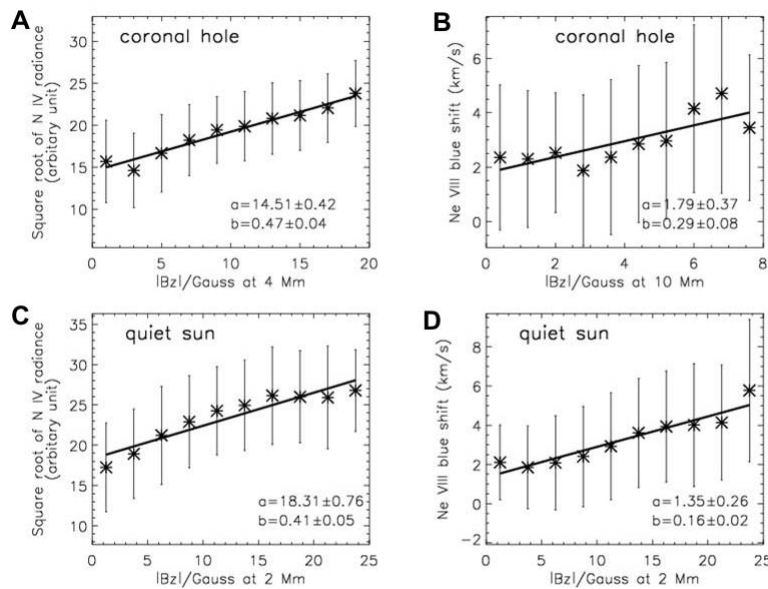
Fig. 8 Dependence of the square root of the radiance of N IV (left), and the blue shift of Ne VIII (right) on $|B_z|$ in the coronal hole (upper) and the quiet Sun (lower) at the respective correlation height. The averages in the bins are indicated by asterisks. The uncertainties show corresponding standard deviations of the averages. The thick solid lines show linear fits to the averages.

Table 3 Parameters of the linear correlation between radiance and $|B_z|$ for the lower-transition-region lines, and between doppler shift and $|B_z|$ for Ne VIII.

Ion	Coronal hole		Quiet Sun	
	a	b	a	b
Ne VIII	1.79 ± 0.37	0.29 ± 0.08	1.35 ± 0.26	0.16 ± 0.02
O V	7.15 ± 0.19	0.24 ± 0.02	9.40 ± 0.46	0.23 ± 0.03
O IV ($\lambda787.710$)	13.45 ± 0.41	0.53 ± 0.04	16.88 ± 0.81	0.44 ± 0.06
O IV($\lambda790.199$)	19.99 ± 0.61	0.78 ± 0.05	25.15 ± 1.22	0.66 ± 0.08
S V	9.62 ± 0.29	0.44 ± 0.03	12.27 ± 0.59	0.35 ± 0.04
N IV	14.51 ± 0.42	0.47 ± 0.04	18.31 ± 0.76	0.41 ± 0.05
N III	3.95 ± 0.13	0.15 ± 0.01	4.88 ± 0.18	0.12 ± 0.01

Figure 7 shows the temperature variations of the correlation heights in both the quiet Sun and the coronal hole region. Since the correlation heights and height ranges of the emissions of the two O IV lines are similar, we only present the result of O IV ($\lambda787.710$). The figure clearly confirmed the concept that plasma with different temperatures can coexist at the same height in the solar transition region (Marsch et al. 2006). In the upper transition region, we see a much higher emission height in the coronal hole, indicating a much stronger expansion of the magnetic structure.

We also carried out a linear fit using the formula $y = a + bx$ to the dependence of the square root the radiance of each middle-transition-region line and the blue shift of Ne VIII (the reverse value of the normal Doppler shift) on $|B_z|$ at the correlation height of each line. The fitting results are presented in Figure 8 and the fitting parameters are listed in Table 3. We found that, for all the six lower-transition-region lines, the square root of radiance increases linearly with $|B_z|$ at the correlation height, which is consistent with the results in Marsch et al. (2006). We calculated the correlation coefficient between the blue shift of Ne VIII and $|B_z|$ at the correlation height in each region, and obtained a value of 0.502 for the coronal hole and

0.948 for the quiet Sun, respectively. This result suggests that the dependence of the blue shift of Ne VIII on magnetic field is much stronger in the quiet Sun than in the coronal hole. If we assume the magnetic fluxes increase steadily from the internetwork region to the network center, then the result in the quiet Sun seems to support our previous finding for the large-blueshift cases in a quiet Sun region that the blue shift of Ne VIII increases almost linearly from the internetwork region to the network center (Tian et al. 2008c).

5 CONCLUSIONS

We analyzed a set observed data by SUMER/*SOHO* in an equatorial coronal hole and the surrounding quiet Sun region, and determined the emission heights for six lower-transition-region lines and an upper-transition-region line Ne VIII, through a correlation analysis between the radiance or Doppler shift and $|B_z|$ as extrapolated from the photospheric magnetogram observed by MDI/*SOHO* to the different heights.

We provided a direct comparison of emission heights of EUV lines in the equatorial coronal hole and the surrounding quiet Sun. The results show that the magnetic field correlates well with the radiance of lower-transition-region lines and the blue shift of Ne VIII. We found the emission heights of the lower-transition-region lines are 4–5 Mm in the coronal hole and around 2 Mm in the quiet Sun region. In the quiet Sun region, the correlation height of Ne VIII is 1.8 Mm, which is not systematically different from that of a lower-transition-region line. However, the correlation height of Ne VIII is 9.8 Mm in the coronal hole.

Our results confirm that plasma with different temperatures can coexist at the same height in the transition region, and reveal clearly that the outflow of Ne VIII is a signature of solar wind in the coronal hole and is just mass supply to large loops in the quiet Sun.

References

Aiouaz T., Peter H., Lemaire P., 2005, A&A, 435, 713
Aiouaz T., 2008, ApJ, 674, 1144
Berger T. E., Lites B. W., 2003, Sol. Phys., 213, 213
Dammasch I. E., Wilhelm K., Curdt W., Hassler D. M., 1999, A&A, 346, 285
Dere K. P., Landi E., Mason H. E., Monsignori-Fossi B. F., Young P. R., 1997, A&AS, 125, 149
Dowdy J. F. Jr., Rabin D., Moore R. L., 1986, Sol. Phys., 105, 35
Feng L., Gan W.-Q., 2006, Chin. J. Astron. Astrophys. (ChJAA), 6, 5, 608
Gabriel A. H., 1976, Philos. Trans. R. Soc. London A, 28l, 575
Hansteen V. H., 1993, ApJ, 402, 741
Hassler D. M., Dammasch I. E., Lemaire P. et al., 1999, Science, 283, 810
He J.-S., Tu C.-Y., Marsch E., 2007, A&A, 468, 307
Landi E., Del Zanna G., Young P. R., Dere K. P., Mason H. E., Landini M., 2006, ApJS, 162, 261
Lemaire P., Wilhelm K., Curdt W. et al., 1997, Sol. Phys., 170,105
Lemaire P., Bocchialini K., Aletti V., Hassler D., Wilhelm K., 1999, Space Sci. Rev., 87, 249
Mariska J. T., 1992, The Solar Transition Region, Cambridge: Cambridge Univ. Press
Marsch E., Wiegelmann T., Xia L.-D., 2004, A&A, 428, 629
Marsch E., Zhou G.-Q., He J.-S., Tu C.-Y., 2006, A&A, 457, 699

Metcalf T. R., Jiao L., McClymont A. N., Canfield R. C., 1995, ApJ, 439, 474
Peter H., 1999, ApJ, 516, 490
Peter H., Judge P. G., 1999, ApJ, 522, 1148
Peter H., 2001, A&A, 374, 1108
Patsourakos S., Vial J.-C., Gabriel A. H., Bellamine N., 1999, ApJ, 522, 540
Reeves E. M., 1976, Sol. Phys., 46, 53
Scherrer P. H., Bogart R. S., Bush R. I. et al., 1995, Sol. Phys., 162,129
Seehafer N., 1978, Sol. Phys., 58, 215
Schrijver C. J., Sandman A. W., Aschwanden M. J., DeRosa M. L., 2004, ApJ, 615, 512
Stucki K., Solanki S. K., Schühle U. et al., 2000, A&A, 363, 1145
Teriaca L., Banerjee D., Doyle J. G., 1999, A&A, 349, 636
Tian H., Tu C.-Y., He J.-S., Marsch E., 2007, Adv. Space Res., 39,1853
Tian H., Tu C.-Y., Marsch E., He J.-S., Zhou G.-Q., 2008a, A&A, 478, 915
Tian H., Marsch E., Tu C.-Y., Xia L.-D., He J.-S., 2008b, A&A, 482, 267
Tian H., Tu C.-Y., Xia L.-D., He J.-S., 2008c, A&A, 489, 1297
Tu C.-Y., Zhou C., Marsch E., Xia L.-D., Zhao L., Wang J.-X., Wilhelm K., 2005a, Science, 308, 519
Tu C.-Y., Zhou C., Marsch E., Wilhelm K., Zhao L., Xia L.-D., Wang J.-X., 2005b, ApJ, 624, L133
Tu C.-Y., Zhou C., Marsch E., Wilhelm K., Xia L.-D., Zhao L., Wang J.-X., 2005c, Proceedings of SW 11-SOHO 16,
    Connecting Sun and Heliosphere, Whistler, Canada, 12-17 June 2005, ESA SP-592
Wang J., Zhou G., Wang Y., Song L., 2003, Sol. Phys., 216, 143
Wiegelmann T., Neukirch T., 2002, Sol. Phys., 208, 233
Wiegelmann T., Xia L.-D., Marsch E., 2005, A&A, 432, L1
Wilhelm K., Curdt W., Marsch E. et al., 1995, Sol. Phys., 162,189
Wilhelm K., Dammasch I. E., Marsch E., Hassler D. M., 2000, A&A, 353, 749
Xia L.-D., Marsch E., Curdt W., 2003, A&A, 399, L5
Xia L.-D., 2003, Ph.D. Thesis, Göttingen: Georg-August-Univ.
Xia L.-D., Marsch E., Wilhelm K., 2004, A&A, 424, 1025